Available online at www.sciencedirect.com

ScienceDirect

Mendeleev Commun., 2023, **33**, 769–773

Mendeleev Communications

Femtosecond absorption spectroscopy of bis-aza-18-crown-6-containing dibenzylidenecyclobutanone complexes with alkali and alkaline-earth metal cations

Valery V. Volchkov,*[a] Mikhail N. Khimich,[a] Mikhail Ya. Melnikov,[a] Fedor E. Gostev,[b] Ivan V. Shelaev,[b] Viktor A. Nadtochenko,[b] Roman O. Starostin,[a,c] Marina V. Fomina,[c] Alexandra Ya. Freidzon[d,e] and Sergey P. Gromov[a,c]

[a] *Department of Chemistry, M. V. Lomonosov Moscow State University, 119991 Moscow, Russian Federation. E-mail: volchkov_vv@mail.ru*
[b] *N. N. Semenov Federal Research Center for Chemical Physics, Russian Academy of Sciences, 119991 Moscow, Russian Federation*
[c] *Photochemistry Centre, FRC 'Crystallography and Photonics', Russian Academy of Sciences, 119421 Moscow, Russian Federation*
[d] *National Research Nuclear University MEPhI, 115409 Moscow, Russian Federation*
[e] *Weizmann Institute of Science, 7610001 Rehovot, Israel*

DOI: 10.1016/j.mencom.2023.10.010

Transient absorption spectroscopy, kinetics of absorption anisotropy decay for bis-aza-18-crown-6-containing dibenzylidenecyclobutanone dye and its metal complexes, and quantum chemical calculations support the presence of the first stage in the photorecoordination mechanism for the complexes with the Ba^{2+}, Ca^{2+}, and K^+ cations. The depolarization parameters, including the radii of solvates, are deduced from the experimental data. During the barrierless photorecoordination of the complex with two Ba^{2+} cations, the solvent shell of the crowned Ba^{2+} cation undergoes the following changes: (2 + 1)MeCN, (3 + 1)MeCN, 4 MeCN.

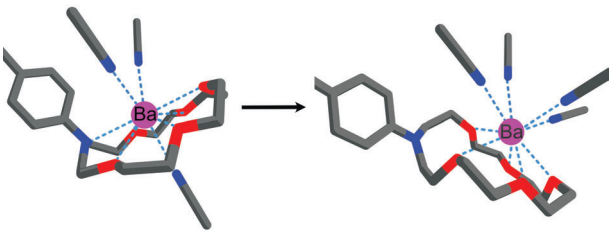

Keywords: aza-18-crown-6, dienones, cyclobutanone, recoordination, alkali, alkaline-earth metal cation, supramolecular complex, TD DFT calculations, time-resolved differential absorption spectroscopy.

Dedicated to M. P. Egorov, Full Member of the Russian Academy of Sciences, on the occasion of his 70th birthday.

Earlier, we reported on the spectral and luminescent behavior of bis-aza-18-crown-6-containing dienone **1**, its supramolecular metal complexes with Ba^{2+}, Ca^{2+}, K^+, Na^+, Li^+, and Mg^{2+} perchlorates in MeCN, and its protonated form $\mathbf{1}\cdot(H^+)_2$ with trifluoroacetic acid.[1] According to the steady-state measurements, the formation of the complex results in the disruption of the quinonoid structure of the dye with the length of the chromophore shortening. The excited complexes of dye **1** with strongly competitive metal cations (Ba^{2+}, Ca^{2+}, and K^+) undergo photoinduced recoordination with the bond between the crowned metal cation and the nitrogen atom of the crown fragment (M–N) becoming significantly weaker or dissociating. The recoordination of the metal cation within the arylazacrown cavity represents a process in which the disruption of bonding between the cation and the nitrogen atom of the crown residue goes in parallel with specific changes in molecular conformation of the macrocycle.[2–5] The most noticeable changes occur for the crowned nitrogen atom: its pyramidal configuration transforms into a flattened form. In addition, a lone pair involved in cation bonding becomes conjugated with the aromatic system of the chromophore. Otherwise, in the initial coordinated conformation the aromatic residue is arranged nearly orthogonally to a mean-square plane of the macrocycle (so called 'axial' conformation). In the recoordinated form this residue is disposed in a plane of the macrocycle ('equatorial' conformation, Scheme 1). It was established, that the presence of an acceptor group in the phenyl ring favors the recoordination in the ground and the excited states. The same influence was observed when the solvent and/or counter ion were able to weaken the interaction between the metal cation and donor atoms of the macrocycle.

We proposed that only one crown group could be involved in recoordination (Scheme 2). It could not be verified whether the final recoordination stage, namely, the ejection of a coordinated metal cation into the bulk solution, occurred in this system. It was reported that the ejection of the metal cation into the solution proceeded for calcium complexes of 2,5-{bis[4*N*-(aza-15-crown-5)phenyl]methylene}cyclopentanone.[6] The photoinduced bond dissociation between the coordinated calcium or lithium

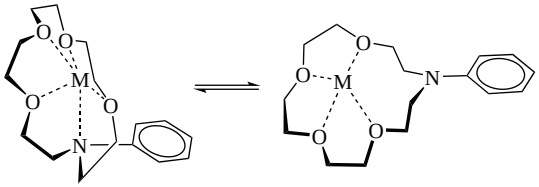

Scheme 1

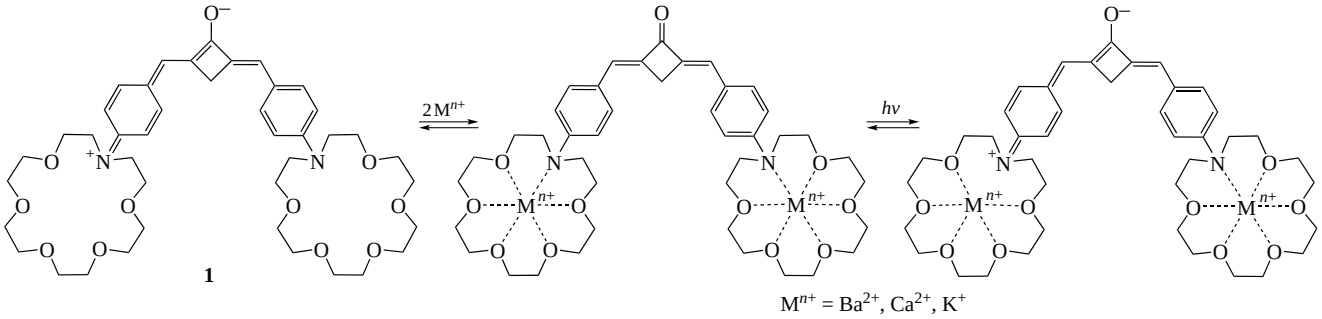

Scheme 2

cations and the nitrogen atom in the crown residue was established for donor–acceptor complexes of merocyanine DCM–azacrown.[7–9] Femtosecond time-resolved differential absorption spectroscopy, anisotropy decay kinetics of S_1–S_n absorption, and quantum chemical (DFT, TD-DFT) calculations provide efficient tools for the analysis of the processes in the excited dienone **1** molecule and its complexes of various stoichiometry (1 : 1, 1 : 2, and 1 : 3). Notably, time-resolved depolarization has not been reported in the analysis of recoordination in metal complexes of crown ethers. Additionally, no prior examples of using ground and excited state conformational curves (total energy of the solvate *vs.* the position of the cation within the crown cavity) could be found. This novel approach provided additional support for our photorecoordination hypothesis, allowing us to estimate its depth, the preferential conformation of the species, and even the solvation type in the excited recoordinated cation.

Compound **1** was synthesized as described elsewhere[7] by alkaline aldol crotonic condensation of cyclobutanone with two molar equivalents of 4′-formylphenylaza-18-crown-6-ether **2** (the Claisen–Schmidt reaction, Scheme 3). Compound **1** was isolated as a brown-red oil, obtained as an *E*,*E*-isomer (NMR spectroscopy data). Indeed, the olefin protons in dienone **1** resonate at 7.01 ppm, which corresponds to the *E*,*E*-isomer.[10]

The transient absorption (TA) spectra (see Online Supplementary Materials) of dye **1** in MeCN contain an intense band with a weak red shift in its maximum (~5 nm) in the 0–1.85 ps range. Concurrently, a strong negative band of stimulated emission (SE) develops at ~600 nm. Up until 500 ps, moderate quenching proceeds for both bands, with their positions and shapes remaining unchanged. Similar behavior is observed for **1**·$(M^{n+})_2$ metal complexes with efficiently bonding cations (Ba^{2+}, Ca^{2+}, and K^+), where each cavity in the crown moiety contains one metal cation. Some differences are observed for the positions of the bands, their emergence times, and for weak (~5 nm) blue shifts in their maxima (Figure 1, Table 1). We used the solutions with excess concentrations of CF_3COOH (0.05 M) as well as Ba (0.02 M) and Ca (0.01 M) perchlorates to achieve ~100 : 1 excess for 1 : 2 *vs.* 1 : 1 complexes. During the spectral evolution of the complexes, no noticeable changes in the shapes and positions of the bands are observed. All arising TA bands are fitted by monoexponential plots (see Figure 1, Table 1). With trifluoroacetic acid as a protonating agent for the nitrogen atom in the crown, an intense short-wavelength band at 410 nm is formed in the range of 0–0.4 ps. After saturation, the band is quenched at 1–10 ps, while a weak long-wavelength band rises at 505 nm. A distinct isosbestic point is observed. Since the protonated form of **1**·$(H^+)_2$ does not fluoresce, the band of stimulated emission is absent.

The TA spectra of the individual **1**·Na^+ (1 : 1) complex and the M^{n+}·**1**·$(M^{n+})_2$ (M^{n+} = Mg^{2+}, Li^+) complexes were recorded as well. The latter are characterized by a red-shifted absorption band in their ground states, allowing for selective excitation. In contrast with the **1**·M^{n+} and **1**·$(M^{n+})_2$ complexes, the red-shifted band of the M^{n+}·**1**·$(M^{n+})_2$ complexes only arises in solutions with large concentrations of perchlorates (>0.1 M). The 1 : 3 complexes contain two crowned metal cations, with the third one being coordinated with the central carbonyl group in the fluorophore. Earlier, the formation of complexes between alkaline-earth metal cations and carbonyl groups was reported for related ketocyanine dyes with no crown ether fragments.[11] The stability constants of these complexes are rather moderate (less than 300 M^{-1}). Generally, the spectral evolution of the TA bands for the M^{n+}·**1**·$(M^{n+})_2$ complexes is similar to that for the **1**·M^{n+}, **1**·$(M^{n+})_2$ complexes.

In our interpretation, after the ultrafast excitation of dye **1** and the metal complexes of all three types, fast vibrational relaxation into the fluorescent S_1 ππ* state occurs. In each case, this state is

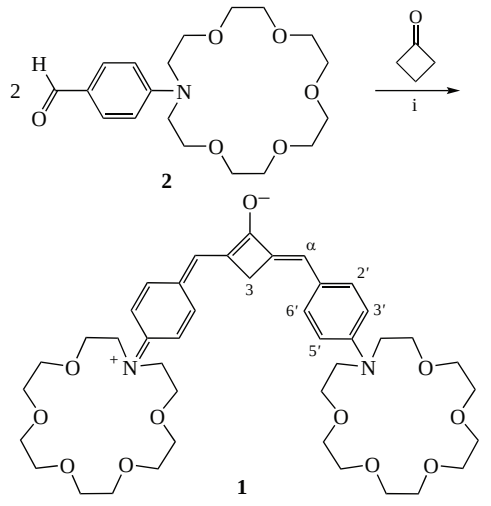

Scheme 3 *Reagents and conditions*: i, NaOH, $EtOH/H_2O$, room temperature.

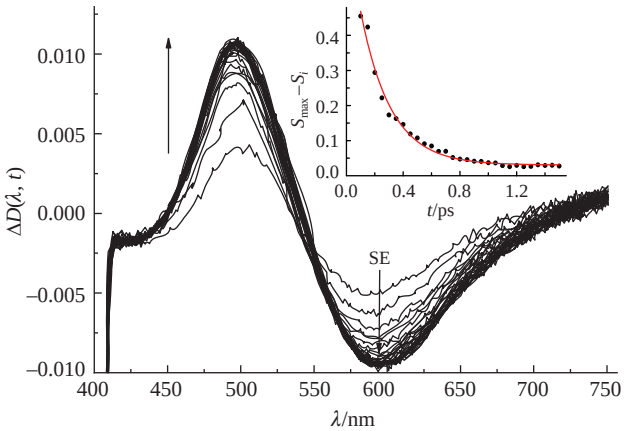

Figure 1 Transient absorption (TA) band and stimulated emission (SE) band of the **1**·$(Ca^{2+})_2$ complex in MeCN (0.15–1.5 ps, increment: 0.05 ps). Inset: TA band kinetics at 496 nm, monoexponential fitting $y = 0.68(-t/0.23)$. Excitation pulse: 40 fs at 401 nm.

Table 1 Spectral-kinetic parameters of the TA spectra for dye **1** and its complexes in MeCN at 295 K.[a]

Sample[b]	λ_a^{max}/nm	λ_{SE}^{max}/nm[c]	τ/ps	r_0	Θ/ps	δ/deg	V_S/Å^3	r_S/Å
1	523	~596	0.43	0.057 ± 0.003	107 ± 8	49.1 ± 0.3	1221 ± 91	6.6 ± 0.2
1·$(Ba^{2+})_2$	504	~598	0.52	0.219 ± 0.002	175 ± 2	33.3 ± 0.2	1997 ± 22	7.8 ± 0.04
1·$(Ca^{2+})_2$	496	~598	0.23	0.192 ± 0.001	264 ± 3	36.1 ± 0.1	3012 ± 34	9.0 ± 0.01
1·Na^+	525	~605	0.49	0.277 ± 0.004	284 ± 7	26.9 ± 0.5	3240 ± 80	9.2 ± 0.07
Mg^{2+}·**1**·$(Mg^{2+})_2$	497	~644	0.13	0.244 ± 0.003	556 ± 17	30.7 ± 0.4	6343 ± 194	11.5 ± 0.1
Li^+·**1**·$(Li^+)_2$	472	~622	0.61	0.219 ± 0.006	319 ± 15	33.3 ± 0.6	3639 ± 172	9.5 ± 0.1
1·K^+ + **1**·$(K^+)_2$[d]	502	~605	0.25	–	–	–	–	–
1·$(H^+)_2$	410, 505	–	0.15, 1.69[e]	0.294 ± 0.004	282 ± 7	24.9 ± 0.5[f]	3206 ± 91	9.2 ± 0.08

[a] λ_a^{max} and λ_{SE}^{max} are the spectral maxima of the TA and SE bands; τ is the characteristic emergence time of the TA band; r_0 is the initial anisotropy; Θ is the characteristic time of anisotropy quenching; δ is the initial angle between the transition absorption moments $M_{(S0\rightarrow S1)}$ and $M_{(S1\rightarrow S2)}$; and V_S and r_S are the volume and radius of the rotating sphere modeling of the fluorophore molecule. All errors in δ, V_S and r_S parameters were determined on a basis of the errors obtained for r_0 and Θ. The latter were obtained by the standard fitting method for monoexponential decay build into Origin 7.0 package. [b] Excitation wavelengths: 350 nm [**1**·$(H^+)_2$]; 401 nm [**1**·$(Ba^{2+})_2$, **1**·$(Ca^{2+})_2$, **1**·K^+ + **1**·$(K^+)_2$]; 403 nm (**1**); 470 nm (**1**·Na^+); and 520 nm [Li^+·**1**·$(Li^+)_2$]; 540 nm [Mg^{2+}·**1**·$(Mg^{2+})_2$]. Excitation pulse, full width at half maximum (FWHM): 40–50 fs. [c] At a 2 ps delay relative to the excitation pulse. [d] Concentration ratio for the 1 : 1 and 1 : 2 complexes in the saturated solution of $KClO_4$ in MeCN (0.0119 M) is equal to ~5 : 3. Due to the inability to excite an individual complex, absorption anisotropy decay kinetics was not measured. [e] Characteristic emergence time for the $S_2\rightarrow S_m$ and $S_1\rightarrow S_n$ absorption bands. [f] Angle between the vectors of absorption transition moments ($S_0\rightarrow S_2$ and $S_2\rightarrow S_m$).

characterized by a single band of $S_1\rightarrow S_n$ absorption. Its position and intensity depend on the type of the complex, the character and degree of charge redistribution in the excited molecule, its prevailing conformation, solvation type, and photorecoordination depth. The pronounced differences in the positions and emergence times of the TA bands for the dye and the complexes allow us to suggest that photorecoordination does not reach its final stage here. The preservation of the positions and shapes of the TA bands for the complexes within the ps time scale indicates that recoordination is completed within hundreds of fs, corresponding with vibrational relaxation times. A small blue shift accompanying the TA band rise for the complexes suggests a more polarized character for **1**·$(M^{n+})_2$ upon its recoordination (see Scheme 2).

The discussed features of the spectral evolution for the **1**·$(H^+)_2$ complex are related to disrupted conjugation between the phenyl group and nitrogen atom in the azacrown ether residue. This results in such a strong blue shift in absorption (1.09 eV) that the actual transition energy (3.69 eV) exceeds the calculated energy of the prohibited dienone-localized $n\rightarrow\pi^*$ transfer (3.03 eV). Thus, under 350 nm excitation, the S_2 state is populated (see Online Supplementary Materials, Figure S1), with a fast vibrational relaxation to the lowest vibrational level of S_2 occurring within ~1 ps. This corresponds to the rise in the observed short-wavelength $S_2\rightarrow S_m$ absorption band. Within the 1–10 ps range, a $S_2\rightarrow S_1$ conversion develops with the $S_2\rightarrow S_m$ band quenched. Concurrently, the $S_1\rightarrow S_n$ band is enhanced (Figures S1 and S2). Both bands demonstrate a distinct 'precursor–successor' relationship, with the position of the $S_1\rightarrow S_n$ band being similar to that for metal complexes.

The absorption anisotropy decay kinetics [$r(t)$, 1–500 ps] was measured to find the depth of recoordination and degree of solvation. We used the solutions of dye **1**, protonated form **1**·$(H)_2$, and three types of complexes: **1**·M^{n+}, **1**·$(M^{n+})_2$, and M^{n+}·**1**·$(M^{n+})_2$. The obtained decay kinetics (Figure 2) was fitted by monoexponential plots, assuming spherical shapes for the molecules. Since the experimental points were widely scattered, the use of polyexponential plots was not justified. The calculated absorption anisotropy kinetic parameters are collected in Table 1: dye **1** shows minimal initial r_0 anisotropy, corresponding to a

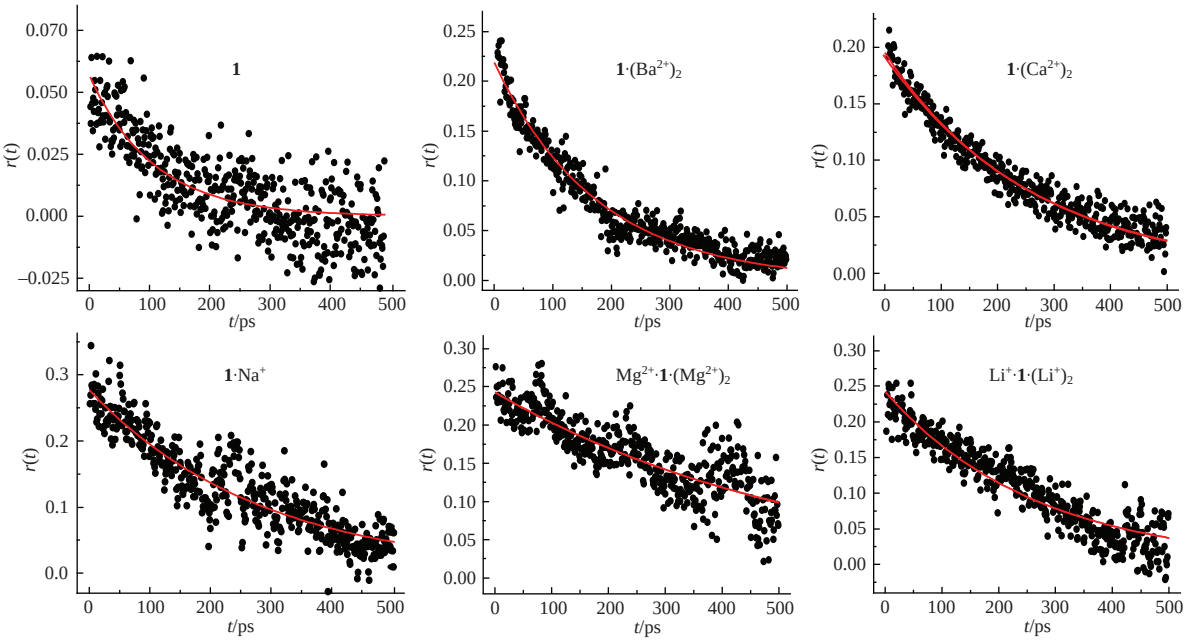

Figure 2 Absorption anisotropy decay kinetics measured at the maxima of the TA bands for dye **1** and the metal complexes. Monoexponential fitting in red: $r(t) = r_0\exp(-t/\Theta)$. The fitting parameters are collected in Table 1. (The TA band areas were not used in the calculations because of a partial overlap between the TA and SE bands.)

large initial δ angle between the vectors of transition moments, $M_{(S0\rightarrow S1)}$ and $M_{(S1\rightarrow S2)}$. Additionally, minimal characteristic time of anisotropy quenching Q is found for dye **1**. The discovered differences between the depolarization parameters of the dye and the complexes point to the metal cation residing within each cavity of the azacrown ether fragment for the duration of the excited state lifetime. In other words, the third recoordination stage does not proceed in all cases. To calculate the depolarization parameters of the solvates, equations (1)–(3) were used:[12]

$$r(t) = \frac{I_{II}(t) - I_{\perp}(t)}{I_{II}(t) + 2I_{\perp}(t)}, \quad (1)$$

$$\delta = \arccos\sqrt{\frac{5r_0 + 1}{3}}, \quad (2)$$

$$V_S = \frac{\Theta kT}{\eta}, \quad (3)$$

where $I_{II}(t)$ and $I_{\perp}(t)$ are the intensity decay plots of the TA band at wavelength λ, measured at the parallel and orthogonal positions of the analyzer relative to the linearly polarized excitation pulse; r_0 and $r(t)$ are the initial and time-resolved absorption anisotropy; Θ is the characteristic time of anisotropy decay; k and T are the Boltzmann constant and absolute temperature (K), respectively; and η is the solution viscosity (3.57×10^{-4} Pa s, MeCN at 293 K).[13]

Equation (3) allowed us to find V_S, the volume of the rotating sphere, and, correspondingly, its radius, r_S (see Table 1). Here, the sphere represents the averaged conformation of the dye or the complex within their nearest solvate shell, rotating as a single entity in Brownian motion. The data demonstrate that the thickness of the solvate shell differs between the dye and the complexes. The highest values of V_S and r_S correspond to the Mg^{2+}·**1**·$(Mg^{2+})_2$ complex, and the lowest ones correspond to the dye itself. The **1**·M^{n+} and **1**·$(M^{n+})_2$ inclusion complexes, where the metal cations are captured by the cavities of the azacrown fragments, are more compact, since their dimensions are closer to those of the dye molecule. Here the increase in the values of V_S and r_S may be explained in terms of structural recoordination: the more compact 'axial' conformation transforms into an elongated 'equatorial' conformation with stronger solvation at the crowned metal cations.[14] The complete photorelaxation pathway for the inclusion complexes is presented in Scheme 4.

According to the steady-state spectroscopy data, photorecoordination manifests itself most dramatically in the **1**·$(Ba^{2+})_2$ complex with its anomalously large Stokes shift for fluorescence (ΔE = 1.3 eV).[1] Thus, our computational approach was initially applied to this test system. According to the calculations, upon excitation, a charge transfer occurs in **1**·$(Ba^{2+})_2$, involving two amino groups as donors and the central carbonyl moiety in the complex as the acceptor. This transfer weakens the $Ba^{2+}\cdots$N coordination bond, with interatomic distance elongating from 3.1 to 4.6 Å. Two dihedral angles (C^1–C–N–C^2 and C^3–C–N–C^4) decrease from 34 to 16° and from 85 to 48°, respectively. Additionally, the pyramidalization degree of the nitrogen atom decreases from 25 to 10°. The partial exit of the Ba^{2+} cation from the crown cavity provokes solvation type changes during

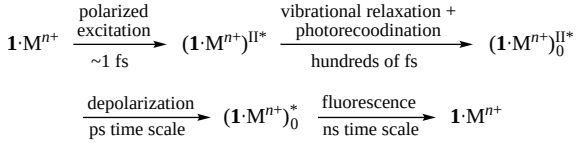

M^{n+} = Ba^{2+}, Ca^{2+}, K^+

Scheme 4

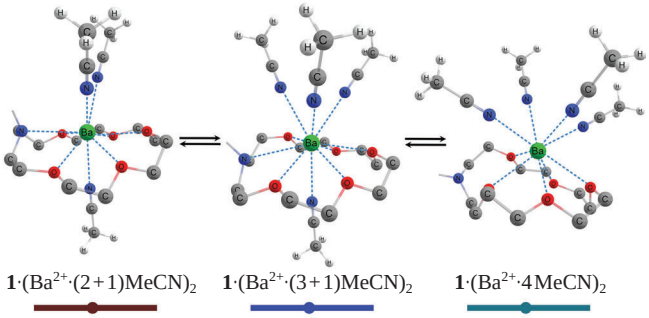

Figure 3 Changes in the nearest solvent shell of the crowned Ba^{2+} cation during the photorecoordination of **1**·$(Ba^{2+})_2$ (lone crown-ether fragment of the complex is shown as a reference, see Online Supplementary Materials for details).

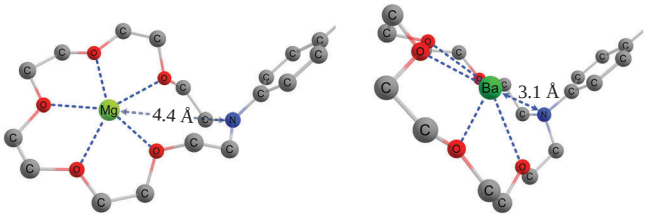

Figure 4 Structural fragments of (left) Mg^{2+}·**1**·$(Mg^{2+})_2$ and (right) **1**·$(Ba^{2+})_2$ complexes in their ground states.

recoordination: (2 + 1) MeCN → (3 + 1) MeCN → (4 + 0) MeCN (Figure 3).

Contrary to the complexes where the dimensions of the metal cation are close to the size of the cavity in the azacrown ether residue, the inclusion complexes with small cations exhibit another type of coordination. The calculation for the ground state of Mg^{2+}·**1**·$(Mg^{2+})_2$ shows that the crowned Mg^{2+} cations are far away from the nitrogen atoms of the substituted amino groups (4.4 Å), *i.e.*, there is no bonding (Figure 4). The amino groups themselves are almost non-pyramidal (angle < 0.2°); the lone pairs on both nitrogen atoms are conjugated with the aromatic system in the complex. Therefore, the partial negative charge on the carbonyl group increases [from –0.19 for **1**·$(Ba^{2+})_2$ to –0.23 for **1**·$(Mg^{2+})_2$], stabilizing the Mg^{2+}·**1**·$(Mg^{2+})_2$ complex.

Calculating the data for conformational curves ascertains the recoordination type in the complexes (Figure 5), illustrating the recoordination process in the ground and excited states of the **1**·$(Ba^{2+})_2$ complex. Apparently, the total energy of the complex decreases only when the Ba–N distance grows concurrently with the changes in the solvent shell type of the Ba^{2+} cation. In this

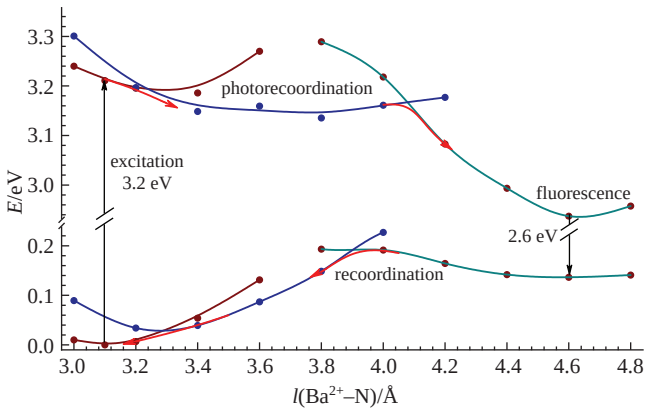

Figure 5 Total energy of the **1**·$(Ba^{2+})_2$ complex as a function of the interatomic Ba–N distance. Arrows depict the possible relaxation pathways. The color of the curves corresponds to the solvent shell type for the crowned Ba^{2+} cation (see Figure 3).

case, photorecoordination is barrierless whereas the reverse process for the ground state has a small barrier. Stronger conjugation in the recoordinated excited state decreases the total energy of the molecule. This finding explains the anomalous bathochromic Stokes shift in the fluorescence of **1**·$(Ba^{2+})_2$.

The actual structures of the dye and the complexes can deviate significantly from the spherical shape; therefore, the measured depolarization parameters are estimates. Nevertheless, they can be used to compare the dimensions of the solvated species. The minimal V_S' and r_S' values (Table S1) correspond to the individual dye molecule. According to our calculations, the molecule of dye **1** is partially twisted, reducing its effective size by a quarter. Additionally, the neutral dye can only form weak bonds with the acetonitrile molecule (acetonitrile is a polar solvent, but it is unable to form hydrogen bonds). The elongated 'equatorial' conformation is typical for the excited molecules of metal complexes. Their solvation is stronger due to the coordination between the MeCN molecule and the crowned metal cations. Therefore, the inclusion complexes of the **1**·M^{n+} and **1**·$(M^{n+})_2$ types should be larger. Thus, the size of the **1**·$(Ba^{2+}\cdot 4\,MeCN)_2$ solvate should exceed the size of **1**·$(Ca^{2+}\cdot 3\,MeCN)_2$ due to longer metal–ligand bonds and a higher number of ligands. It is confirmed by our calculations: the volume of **1**·$(Ba^{2+}\cdot 4\,MeCN)_2$ exceeds the volume of **1**·$(Ca^{2+}\cdot 3\,MeCN)_2$ and is close to that of **1**·$(Mg^{2+}\cdot 2\,MeCN)_2$·$(Mg\cdot 5\,MeCN)$ (see Table S1). On the other hand, the characteristic time of absorption anisotropy decay kinetics for the solvate of **1**·$(Ba^{2+})_2$ is noticeably lower (see Table 1). This discrepancy can be attributed to the differences in the thicknesses of the nearest solvent shells rotating with the complexes as single entities. For the same reasons, the Θ values of the Mg^{2+}·**1**·$(Mg^{2+})_2$ and Li^+·**1**·$(Li^+)_2$ complexes differ, although their dimensions are close. Naturally, having a fourfold larger charge density than Li^+, the Mg^{2+} cation forms stronger bonds with the azacrown ether residues, the carbonyl group of cyclobutanone, as well as acetonitrile, producing a larger and more stable solvent shell. Structure of the Mg^{2+}·**1**·$(Mg^{2+})_2$ complex is shown in Figure S4. The 'equatorial' conformations are absent for the aza-18-crown-6 complexes with small Mg^{2+} and Li^+ cations. The calculation confirms a possibility to coordinate the third metal cation to carbonyl oxygen. In our recent paper dedicated to supramolecular metal complexes of (*E*)-bis(18-crown-6)azobenzene, we posited that the most stable conformation of the complex should contain from 4 (for Ca^{2+}) to 6 (for K^+) solvent molecules forming the first coordination sphere of the metal cation located within the cavity of the azacrown ether residue.[15]

A novel approach combining time-resolved TA measurements with quantum chemical calculations allows one to confirm the presence of the first photorecoordination stage for the metal complexes of different stoichiometry (1 : 1, 1 : 2, and 1 : 3) formed by bis-aza-18-crown-6-containing cyclobutanone with Ba^{2+}, Ca^{2+}, and K^+ cations. The process takes no more than hundreds of fs; no photoejection of any metal cation can be observed up to 500 ps. On the basis of the plotted conformation curves the whole recoordination cycle for the **1**·$(Ba^{2+})_2$ complex is described in details. An actual energy relaxation pathway including a recoordination stage is proposed for the studied metal complexes. It was demonstrated that the volumes of the solvates [excluding **1**·$(Ba^{2+})_2$] measured in the absorption anisotropy decay kinetics correspond to those obtained from quantum chemical calculations. The lower experimental V_S value obtained for **1**·$(Ba^{2+})_2$ can be attributed to the additional channel of structural relaxation in this complex.

This work, excluding its synthetic part, was supported by the Russian Science Foundation (grant no. 22-23-00161). The development of synthetic approaches to bis-aza-18-crown-6-containing dibenzylidenecyclobutanone was supported by the Russian Science Foundation (grant no. 22-23-00064). Quantum chemical calculations were carried out using the equipment of the shared research facilities of HPC computing resources at Lomonosov Moscow State University.[16]

Online Supplementary Materials

Supplementary data associated with this article can be found in the online version at doi: 10.1016/j.mencom.2023.10.010.

References

1 V. V. Volchkov, M. N. Khimich, M. Ya. Melnikov, A. E. Egorov, R. O. Starostin, M. V. Fomina and S. P. Gromov, *Mendeleev Commun.*, 2023, **33**, 380.
2 A. Ya. Freidzon, A. A. Bagatur'yants, S. P. Gromov and M. V. Alfimov, *Russ. Chem. Bull.*, 2003, **52**, 2646 (*Izv. Akad. Nauk, Ser. Khim.*, 2003, 2505).
3 A. Ya. Freidzon, A. A. Bagatur'yants, S. P. Gromov and M. V. Alfimov, *Int. J. Quantum Chem.*, 2004, **100**, 617.
4 A. Ya. Freidzon, A. A. Bagatur'yants, S. P. Gromov and M. V. Alfimov, *Russ. Chem. Bull.*, 2005, **54**, 2042 (*Izv. Akad. Nauk, Ser. Khim.*, 2005, 1981).
5 A. Ya. Freidzon, A. A. Bagatur'yants, S. P. Gromov and M. V. Alfimov, *Russ. Chem. Bull.*, 2008, **57**, 2045 (*Izv. Akad. Nauk, Ser. Khim.*, 2008, 2009).
6 N. Marcotte, P. Plaza, D. Lavabre, S. Fery-Forgues, and M. M. Martin, *J. Phys. Chem. A*, 2003, **107**, 2394.
7 M. M. Martin, P. Plaza, N. Dai Hung, Y. H. Meyer, J. Bourson and B. Valeur, *Chem. Phys. Lett.*, 1993, **202**, 425.
8 M. M. Martin, P. Plaza, Y. H. Meyer, F. Badaoui, J. Bourson, J. P. Lefevre and B. Valeur, *J. Phys. Chem.*, 1996, **100**, 6879.
9 P. Plaza, I. Leray, P. Changenet-Barret, M. M. Martin and B. Valeur, *ChemPhysChem*, 2002, **3**, 668.
10 M. V. Fomina, A. Ya. Freidzon, L. G. Kuz'mina, A. A. Moiseeva, R. O. Starostin, N. A. Kurchavov, V. N. Nuriev and S. P. Gromov, *Molecules*, 2022, **27**, 7602.
11 J. K. Basu, M. Shannigrahi and S. Bagchi, *J. Phys. Chem. A*, 2007, **111**, 7066.
12 J. R. Lakowicz, *Principles of Fluorescence Spectroscopy*, 3rd edn., Springer, Berlin, 2006.
13 I. T. Goronovsky, Yu. P. Nazarenko and E. F. Nekryach, *Kratkii spravochnik po khimii (A Short Guide to Chemistry)*, Naukova Dumka, Kiev, 1983 (in Russian).
14 A. Ya. Freidzon, K. G. Vladimirova, A. A. Bagatur'yants, S. P. Gromov and M. V. Alfimov, *J. Mol. Struct: THEOCHEM*, 2007, **809**, 61.
15 A. A. Granovsky, *Firefly 8.2, Build 10203*, 2017.
16 V. V. Voevodin, A. S. Antonov, D. A. Nikitenko, P. A. Shvets, S. I. Sobolev, I. Yu. Sidorov, K. S. Stefanov, V. V. Voevodin and S. A. Zhumatiy, *Supercomput. Front. Innov.*, 2019, **6** (2), 4.

Received: 5th June 2023; Com. 23/7182